Published in final edited form as:
Nano Lett. 2012 August 8; 12(8): 4117–4123. doi:10.1021/nl301655d.

Assessing Graphene Nanopores for Sequencing DNA

David B. Wells, **Maxim Belkin**, **Jeffrey Comer**, and **Aleksei Aksimentiev***
Department of Physics, University of Illinois, 1110 W. Green St., Urbana, IL

Abstract

Using all-atom molecular dynamics and atomic-resolution Brownian dynamics, we simulate the translocation of single-stranded DNA through graphene nanopores and characterize the ionic current blockades produced by DNA nucleotides. We find that transport of single DNA strands through graphene nanopores may occur in single nucleotide steps. For certain pore geometries, hydrophobic interactions with the graphene membrane lead to a dramatic reduction in the conformational fluctuations of the nucleotides in the nanopores. Furthermore, we show that ionic current blockades produced by different DNA nucleotides are, in general, indicative of the nucleotide type, but very sensitive to the orientation of the nucleotides in the nanopore. Taken together, our simulations suggest that strand sequencing of DNA by measuring the ionic current blockades in graphene nanopores may be possible, given that the conformation of DNA nucleotides in the nanopore can be controlled through precise engineering of the nanopore surface.

Keywords

Nanopore; graphene; molecular dynamics; biosensors; nucleic acids; ionic current

The idea of using a nanopore to sequence DNA[1] has generated much excitement since DNA translocation through the biological nanopore α-hemolysin was first demonstrated.[2] The principle of nanopore sequencing, illustrated in Figure 1, is straightforward: an external electric field is used to drive negatively charged DNA through a nanopore. As DNA transits the pore, its nucleotide sequence is determined by measuring changes in the nanopore ionic current. By reading the sequence directly from genomic DNA, nanopore methods promise to offer single-molecule, label-free DNA sequencing with virtually unlimited read lengths,[3,4] overcoming many of the drawbacks of so-called next-generation sequencing platforms.[5,6]

Spectacular progress in engineering the biological nanopores α-hemolysin[7,8] and MspA[9,10] for sequencing applications indicate the imminent arrival of nanopores in practical biomedical applications.[11] The key factors enabling DNA sequencing using biological nanopores are the nanometer dimensions of the ion-current-modulating regions of the nanopores and the use of processive enzymes to produce DNA translocation in discrete steps.[12,13] Solid-state nanopores[14] offer a number of practical advantages over their biological counterparts, including superior mechanical properties,[15] multiplex detection,[16] integration with on-chip electronics,[17] and detection modalities other than ionic current.[18–25] However, conventional synthetic membranes are generally over 10 nm thick, meaning the

*To whom correspondence should be addressed: aksiment@illinois.edu.

Supporting Information Available: Detailed description of the simulation and analysis methods; plots of the water density in several nanopores; plots characterizing translocation of ssDNA through six nanopores; plots of the number of DNA bases within the pore; plots characterizing DNA adhesion to the surface of a nanopore; graphical definition of vectors used to define the orientation of DNA bases; plots of the ionic currents resulting from MD and BD simulations; animations illustrating MD trajectories. This material is available free of charge via the Internet at http://pubs.acs.org/.

pore is occupied by many DNA bases at the same time, and thus making single-base-sensitive measurements extremely difficult.[4]

The advent of graphene[26]—a single layer carbon sheet—has opened a new chapter in the development of solid-state nanopores for DNA sequencing, with several groups already reporting measurements of ionic current blockades produced by transport of double-stranded DNA through graphene nanopores.[27–30] Graphene nanopores share many advantages of conventional solid-state nanopore systems while offering atomically precise control over the nanopore dimensions, in particular the membrane thickness, which can be of the same order as the distance between neighboring DNA nucleotides in a DNA strand.[27] Furthermore, the unique physical properties of graphene membranes offer several possibilities for DNA sequence detection, including transverse tunneling,[31–33] nanoribbon conductance[34,35] and mechanical deformation of DNA[36,37]

In this letter, we assess the suitability of graphene nanopores for sequencing DNA by measuring ionic current—the method used to detect DNA sequences in the case of biological nanopores.[8,12,13] Using all-atom molecular dynamics (MD)[38] and atomic-resolution Brownian dynamics (BD),[39] we simulate the translocation of single-stranded DNA (ssDNA) through graphene nanopores and characterize the ionic current blockades produced by DNA nucleotides. We show that graphene nanopores have the features that made biological nanopores amenable to sequencing applications: translocation of ssDNA can occur in single-nucleotide steps and the ionic current blockades can be indicative of the type of DNA nucleotides.

To simulate the electric field-driven transport of ssDNA through graphene nanopores, we built several all-atom systems, each containing a graphene membrane with a single nanopore in it, a single DNA strand threaded through the nanopore, and 1 M KCl solution. The systems were simulated using the all-atom MD method,[38] applying a constant electric field normal to the graphene membrane to produce transport of ssDNA and ions through the nanopore. In such classical simulations, the graphene layer serves merely as a barrier to ion passage, which is an adequate approximation to determine general features of ssDNA and ion transport, but may be not accurate enough to yield precise quantitative insights. A complete description of our simulation protocols is given in the Supporting Information. A number of pore sizes, pore shapes, membrane thicknesses, and DNA sequences were examined. Table Table 1 lists all of our production simulations.

Figure 2a illustrates a typical simulation trajectory. In all of our simulations, ssDNA was observed to stick to the surface of the graphene membrane. Although we began our simulations with ssDNA in a conformation extended away from the graphene membrane, within ~25 ns most DNA bases in most systems were found to be in contact with the graphene membrane. Such adsorption of DNA bases has a hydrophobic origin, as water is excluded from the DNA-graphene contact area.[40,41] Despite the strong interaction, DNA remained highly mobile at the graphene surface, performing a kind of two-dimensional diffusion. In likely experimental scenarios, the cross sectional area of the graphene nanopore is negligible in comparison to the area of the graphene membrane; therefore, the most probable sequence of events is that the ssDNA first adsorbs to graphene membrane surface from bulk solution and then enters the nanopore by diffusion along the graphene surface.

Our simulations suggest that such 2D diffusion of ssDNA does not limit the rate of ssDNA translocation through the nanopore. In Figure 2b, we plot the diffusivity of DNA bases adsorbed to one of the graphene surfaces versus the distance from the nanopore, calculated separately for the radial and tangential directions. Near the pore, the tangential diffusivities are seen to be approximately 10 times higher than the radial diffusivities, and both values

increase with the distance from the pore, approaching the free-solution value of ~10 $Å^2$/ns. In the case of the pore featured in Figure 2a, the mean time per base translocation $\bar{t}$ is ~16 ns at a 500 mV bias. Using a conservative estimate for the 2D diffusion coefficient of a DNA base (4 $Å^2$/ns), the expected mean-square displacement of the base within the time interval $\bar{t}$ exceeds the distance between neighboring nucleotides in a DNA strand (~5 Å).

All pores examined in this study remained filled with water during our MD simulations. Figure S1 shows the average water densities along a line passing through the center of the pores normal to the membrane (z-axis in our setup). Some small deviations from the bulk value of 0.1 atoms/$Å^3$ can be seen in the water density profiles near the center of the graphene membrane ($z = 0$). However, when DNA atoms are included in the density calculations, the deviations become considerably smaller, indicating that the water deficit is due to displacement by DNA. Thus, we did not observe ion current gating produced by electric field-induced wetting-dewetting transitions that was experimentally observed for larger hydrophobic pores.[42,43] We hypothesize that the presence of a hydrophilic DNA backbone in the nanopore suppresses such dewetting transitions for the pore geometries considered.

In all simulations, ssDNA was observed to either translocate in steps or not to translocate at all. The latter may be interpreted as a long step, given the limited timescale of our MD simulations ($<$500 ns). For each pore studied, simulations were performed using poly(dA), poly(dC), poly(dG), and poly(dT) homopolymers. In general, the greatest number of nucleotide translocation events were observed for the poly(dT) systems, and the fewest for poly(dG).

The pore diameters explored in our MD simulations ranged from 10.8 to 16 Å. We considered such small pores as they were expected to exhibit deeper ionic current blockades and, possibly, larger sensitivity of the blockade ionic current to the type of DNA nucleotides confined in the pores. Although experimental observations of DNA translocation through such small pores have not yet been reported, recent advances in nanopore fabrication methods[44] suggest that such experiments will soon become possible to carry out. However, our smallest pores proved to be so small that ssDNA would not translocate except at a very high bias (~ 2 V). In addition to circular pores, we also investigated elliptical pores (III, IV, and VI) to determine whether such pores could enhance the ionic current signal by reducing the pore's cross-sectional area and control the DNA conformation by breaking the rotational symmetry of the system. By design, the pores were only large enough for bases to transit when properly aligned. However, rather than steering the DNA, the pores tended to jam, severely limiting conformational fluctuations of ssDNA and thus preventing translocation. Animation M3, illustrating one such MD trajectory, is provided in the Supporting Information. It is possible that at lower electric biases the DNA would be able to more fully explore conformational space and sample conformations which would allow it to translocate. For larger diameter pores, we expect the strong interactions between the graphene membrane and the bases of ssDNA to remain the limiting factor determining the overall speed of ssDNA translocation. Note that the transmembrane biases explored in this study are generally higher than those used in experiments.

We found that the transmembrane bias can affect not only the rate of DNA translocation, but also its qualitative character. Higher biases, such as those used in the smallest pores, generally increased the DNA translocation rate. However, increasing the bias was observed to increase the amount of "skips", i.e. rapid translocation of multiple nucleotides. Animation M4 provided in the Supporting Information shows an example of such skipping. In the case of elliptical pores, a higher bias may also, somewhat paradoxically, lead to slower

translocation due to frustration, by trapping the DNA in a conformation unfavorable for translocation.

Figure 3 compares the results of our MD simulations performed using graphene membranes containing one, two or three carbon layers and the same pore size. The figure shows data for poly(dT)$_{20}$, which is representative of the data obtained using other sequences in pores II, V, and VII; complete translocation data for all systems is provided in Figure S2.

In our one-layer systems, Figure 3a, translocation of ssDNA did not reliably occur in single-nucleotide steps, see Figure 3d and Figure S2b. Because the single layer graphene is only one carbon atom thin, the fraction of time that the pore is occupied by a DNA base is quite small (~ 36%, see Figure S3), which severely limits detection of the DNA sequence by measuring the ionic current. Furthermore, we do not expect that lowering the transmembrane bias would significantly increase the time DNA bases are exposed to the nanopore volume. Instead, lowering the bias is expected to increase the time ssDNA spends between the steps, during which no base occupies the pore (see below).

For a two-layer membrane at same transmembrane bias of 500 mV (Figure 3b), translocation of ssDNA was observed to occur at a higher rate than in the one-layer system (Figure 3d). Although clear single-base steps can be discerned from the DNA translocation trace, there are also many skips. The arrow in Figure 3d indicates one such event: the number of translocated nucleotides rapidly changes from ~4 to ~6 within ~2 ns. In contrast, translocation of ssDNA in the three-layer systems, Figure 3c, was observed to occur predominantly in single-base steps for all four homopolymers sequences studies, Figure 3d–g. In the case of poly(dG) (Figure 3g), translocation was observed only after the transmembrane bias was increased to 800 mV (the translocation was stalled at 500 mV), producing a clearly stepwise translocation pattern in single-base steps. Together, single-base steps accounted for 54% (20/37) of all translocated nucleotides in the pore VII systems, while in the pore II and pore V systems they accounted for 40% (4/10) and 29% (6/21), respectively. Thus, translocation in pore VII was not exclusively in single-base steps; the data for poly(dA) in particular (Figure 3e) show some skipping and continuous translocation. Nevertheless, no other pore that we examined reliably produced single-base steps across all sequences. Overall, the rate of ssDNA translocation was not found to exhibit a simple dependence on the number of carbon layers in a graphene membrane.

The microscopic mechanics of stepwise translocation can be discerned from Figure 3a–c and the animations provided in the Supporting Information. Typically, one translocation step involves unbinding of a DNA base from one side of a graphene membrane and subsequent binding of the same base to the other side of the membrane (single-layer graphene), or concerted unbinding/binding of several neighboring nucleotides (two- and three-layer membranes). In both cases, stepwise transport occurs simultaneously with sliding of the DNA strand along the surface of the membrane. Thus, the microscopic mechanism of stepwise transport appears to involve voltage-dependent barrier crossing events. Therefore, one can expect to considerably reduce the overall rate of ssDNA transport by reducing the transmembrane bias, as the latter should not dramatically affect hydrophobic sticking of DNA bases to graphene. For nanopores in two- and three-layer membranes, more often than not only one base occupies the nanopore, see Figure S3. Furthermore, due to strong hydrophobic interaction, the base occupying the nanopore is localized near its surface, see Figure S4.

The combination of stepwise translocation and localization near the nanopore surface results in a radical reduction of the number of conformations a nucleotide can adopt in the nanopore. To illustrate this point, in Figure 4a–d we plot the z coordinate of the center of

mass of each base versus time using the MD trajectories obtained for pore VII. The plots display the hallmark of stepwise translocation we seek: long stable periods during which a measurement can be performed, punctuated by short periods of DNA translocation to advance to the next base. For each DNA sequence, the histograms of the nucleotide coordinates (Figure 4e–h) display one or two peaks near the membrane center ($z = 0$), highlighting repetitive positioning of DNA bases within the pore. Thus, single bases residing within pore VII are localized both radially (with respect to the pore axis) and longitudinally (along the pore axis). Animations M5–M8 in the Supporting Information illustrate the translocation trajectory of each DNA homopolymer.

Furthermore, the bases adsorbed to the nanopore surface are seen to adopt a limited number of conformations. In Figure 4j we plot a scatter diagram of the angles β and γ, which we use to describe the orientation of a DNA base adsorbed to the nanopore surface. The angle β measures the tilt of the base relative to the membrane, while the angle γ measures the rotation of the base within the plane defined by β; these angles are shown in Figure 4k and defined precisely in Figure S5. The observed orientations fall into two distinct clusters, centered at $(\beta;\gamma) \approx (80°;160°)$ and (65°;295°). The two clusters correspond to conformations that feature the plane of the bases oriented almost parallel to the pore axis (and the nanopore surface) and the two possible flips of the base about the backbone, see Figure 4k. Moreover, the purine and pyrimidine bases were found to display statistically distinct conformations, illustrated in Figure 4l. The clustering of base orientations is indicative of consistent positioning of DNA nucleotides within the nanopore, which is expected to facilitate sequencing due to the dramatic reduction of conformational noise.[45]

As coordinates of every ion in the simulation system are known, the ionic current flowing through the nanopore can be easily determined.[38,46] Typically, we find the open-pore ionic currents I_0 to be in the range of several nanoamperes and the average relative blockade current I/I_0 to range between 12 and 63%, see Table 1. For pores II, V, and VII, which showed consistent DNA translocation, the blockade current was about 60% of the open pore current. The open-pore current, in general, was found to scale with the pore diameter. However, due to the finite size of an ion hydration shell, the effective diameter of the pore for ion transport is smaller than the pore diameter determined using coordinates of carbon atoms.

Predicting the sequence-specific ionic current directly from all-atom MD simulations requires trajectories that greatly exceed the duration of those described in this work. We illustrate this point in Figure S6 by plotting the ion current traces and the normalized current histograms for our MD simulations of pore VII and all four DNA homopolymers. The stochastic variations in the current are too large to draw statistically sound conclusions. Therefore, we chose to estimate the sequence-specific difference in ionic current blockades using our recently developed atomic-resolution Brownian dynamics (ARBD) method.[47] This method allows one to determine the nanopore ionic current to an arbitrary accuracy by using three-dimensional potential of mean force (PMF) maps computed using all-atom MD for all pairs of DNA nucleotides and ionic species (see Figure S7d for an example). Currently, such ARBD simulations neglect conformational fluctuations (the PMF maps are static), which corresponds to the physical situation where the conformational degrees of freedom are reduced to several states, a situation consistent with our observations of ssDNA translocation kinetics in graphene nanopores, see Figure 4.

Since the graphene nanopores in our MD simulations were most often occupied by a single base (see Figure S3), our BD simulations focus on the ionic current signatures of individual nucleotides in a graphene nanopore. In Figure 5, we plot the results of our ARBD simulations for five representative conformations O_1–O_5 of single A, G, C, mC, and T

nucleotides placed in the center of a 24 Å diameter phantom pore at transmembrane biases of +200 and −200 mV, with 50 simulations in total. Orientations O_1–O_3 are model conformations, while O_4 and O_5 represent the most probable conformations seen in our MD simulations; Table S1 in the Supporting Information lists the orientation of the DNA bases in terms of the angles β and γ introduced above. Each simulation was performed with a 1.7 M KCl concentration and lasted about 9 μs. The results of variations on these conditions, using 0.1 M KCl or a ± 600 mV bias, are reported in Figure S8 and Figure S9, respectively.

For a given conformation in the set O_1–O_3, each of the five DNA nucleotides has the same set of backbone coordinates; therefore, the difference seen in the ionic currents is solely due to the difference in the chemical structure of the nucleobases. Nucleotides in conformation O_1 have the greatest cross-section with respect to the direction of the applied electric field and, therefore, yield the lowest current. In this orientation, C and mC nucleotides can be distinguished from A, G and T with $>$95% confidence. In conformations O_2 and O_3, the plane of the nucleobase is perpendicular to the plane of the membrane ($\beta = 90°$). The largest currents are observed in conformation O_2, which has the smallest cross section along the pore axis. In this conformation, the current for thymine (T) prominently lower than the others. At +200 mV one can distinguish methylated cytosine (mC) from A, G and T, but not from C. In conformation O_3, purines (A and G) can be distinguished from pyrimidines (C, mC, T), but the type of purine nucleotides cannot be determined. At +200 mV, T can be distinguished from C and mC. For the systems considered, we found the ion concentration and bias to have little influence on distinguishability of DNA nucleotides by their relative current blockades, see Figure S8 and Figure S9.

In conformations O_4 and O_5, purine and pyrimidine nucleotides have different backbone coordinates (the backbone coordinates are the same within the respective groups). For O_4 at +200 mV, all current blockades are the same within the error, but under a reversed bias, C and mC can be identified as having the highest currents. Furthermore, G can be distinguished from all other nucleotides as having the lowest current. In conformation O_5 (Figure 5e), T can be recognized from other nucleotides at both values of the bias. At a positive bias, the current blockade for A is smaller than for G and C. By reversing the polarity of the applied bias, one can identify G as the one producing the highest current. Thus, all nucleotides except for the C-mC pair in conformation O_5 can be discriminated from each other based on the relative blockade current. In absolute terms, the difference between between A and C in orientation O_4 at −200 mV is roughly 200 pA.

Thus, we have shown that ssDNA translocation through nanopores in graphene membranes may exhibit the same features that have made biological nanopores amenable to DNA sequencing applications. We have found that translocation of ssDNA may proceed in single nucleotide steps, akin to ssDNA translocation controlled by a polymerase motor.[12,13] Hydrophobic adhesion of nucleobases to graphene reduces the likely ssDNA conformations to a few states, which can be sequence specific. Finally, the ionic current blockades produced by immobilized DNA nucleotides may be sufficiently different to identify their type via ionic current measurement, which may involve measurements under alternating electric field. Our simulations suggest that multilayer graphene membranes might be better suited to DNA sequence detection via ionic current measurement than single layer graphene, although one might have to use a hidden Markov chain base-calling method[48] to deconvolve the ionic current trace.

Our simulations also revealed potential problems with the approach. The transport of ssDNA is not always stepwise or even unidirectional and the duration of the steps is stochastic, which can lead to insertion and deletion errors in sequence determination. To optimize control of ssDNA stepping through graphene nanopores, one must minimize zero-bias

displacements of a DNA strand in the nanopore. Given the exponential dependence of the probability of barrier crossing on applied force, controlled stepwise transport of ssDNA might be realized by pulsing the applied electric field. From the limited number of nucleotide conformations examined, we found the blockade current to depend to the same degree or even more on the conformation of nucleotides as on their chemical structure. Through precise chemical decoration of the nanopore surface,[49] one may enhance the resolution of ionic current blockades by engineering sequence-dependent binding of nucleotides in the conformations that enable detection of the bound nucleotides.

Supplementary Material

Refer to Web version on PubMed Central for supplementary material.

Acknowledgments

This work was supported by the grants from the National Science Foundation (DMR-0955959) and the National Institutes of Health (R01-HG005115 and P41-RR005969). The authors gladly acknowledge supercomputer time provided through XSEDE Allocation grant MCA05S028 and the Taub Cluster (UIUC). A.A. would like to thank the Department of Bionanosciences at the Delft University of Technology for hospitality and support from the Netherlands Organisation for Scientific Research (NWO).

References

1. Deamer D, Akeson M. Trends Biotech. 2000; 18:147–151.
2. Kasianowicz JJ, Brandin E, Branton D, Deamer DW. Proc Natl Acad Sci USA. 1996; 93:13770–13773. [PubMed: 8943010]
3. Branton D, et al. Nature Biotech. 2008; 26:1146–1153.
4. Venkatesan BM, Bashir R. Nature Nanotech. 2011; 6:615–624.
5. Metzker M. Nat Rev Genet. 2010; 11:31–46. [PubMed: 19997069]
6. Niedringhaus T, Milanova D, Kerby M, Snyder M, Barron A. Anal Chem. 2011; 83:4327. [PubMed: 21612267]
7. Clarke J, Wu H, Jayasinghe L, Patel A, Reid S, Bayley H. Nature Nanotech. 2009; 4:265–270.
8. Stoddart D, Maglia G, Mikhailova E, Heron A, Bayley H. Angew Chem Int Ed. 2010; 122:566–569.
9. Derrington I, Butler T, Collins M, Manrao E, Pavlenok M, Niederweis M, Gundlach J. Proc Natl Acad Sci USA. 2010; 107:16060. [PubMed: 20798343]
10. Manrao E, Derrington I, Pavlenok M, Niederweis M, Gundlach J. PLoS ONE. 2011; 6:e25723. [PubMed: 21991340]
11. Oxford Nanopores. 2012. http://www.nanoporetech.com/news/press-releases/view/39
12. Cherf G, Lieberman K, Rashid H, Lam C, Karplus K, Akeson M. Nature Biotech. 2012; 30:344–348.
13. Manrao E, Derrington I, Laszlo A, Langford K, Hopper M, Gillgren N, Pavlenok M, Niederweis M, Gundlach J. Nature Biotech. 2012; 30:349–353.
14. Dekker C. Nature Nanotech. 2007; 2:209– 215.
15. Striemer CC, Gaborski TR, McGrath JL, Fauchet PM. Nature. 2007; 445:749–753. [PubMed: 17301789]
16. Kim MJ, Wanunu M, Bell C, Meller A. Adv Mater. 2006; 18:3149–3153.
17. Rosenstein J, Wanunu M, Merchant C, Drndic M, Shepard K. Nature Meth. 2012; 9:487–492.
18. Lagerqvist J, Zwolak M, Ventra MD. Nano Lett. 2006; 6:779–782. [PubMed: 16608283]
19. Zwolak M, Di Ventra M. Rev Mod Phys. 2008; 80:141–165.
20. Gracheva ME, Xiong A, Aksimentiev A, Schulten K, Timp G, Leburton J-P. Nanotechnology. 2006; 17:622–633.
21. Sigalov G, Comer J, Timp G, Aksimentiev A. Nano Lett. 2008; 8:56–63. [PubMed: 18069865]

22. McNally B, Singer A, Yu Z, Sun Y, Weng Z, Meller A. Nano Lett. 2010; 10:2237–2244. [PubMed: 20459065]
23. Huang S, He J, Chang S, Zhang P, Liang F, Li S, Tuchband M, Fuhrmann A, Ros R, Lindsay S. Nature Nanotech. 2010; 5:868–873.
24. Tsutsui M, Taniguchi M, Yokota K, Kawai T. Nature Nanotech. 2010; 5:286–290.
25. Xie P, Xiong Q, Fang Y, Qing Q, Lieber CM. Nature Nanotech. 2012; 116:119–125.
26. Novoselov K, Geim A, Morozov S, Jiang D, Zhang Y, Dubonos S, Grigorieva I, Firsov A. Science. 2004; 306:666. [PubMed: 15499015]
27. Garaj S, Hubbard W, Reina A, Kong J, Branton D, Golovchenko JA. Nature. 2010; 467:190–193. [PubMed: 20720538]
28. Schneider GF, Kowalczyk SW, Calado VE, Pandraud G, Zandbergen HW, Vandersypen LMK, Dekker C. Nano Lett. 2010; 10:3163–3167. [PubMed: 20608744]
29. Merchant CA, Healy K, Wanunu M, Ray V, Peterman N, Bartel J, Fischbein MD, Venta K, Luo Z, Johnson ATC, Drndic M. Nano Lett. 2010; 10:2915–2921. [PubMed: 20698604]
30. Venkatesan BM, Estrada D, Banerjee S, Jin X, Dorgan VE, Bae MH, Aluru NR, Pop E, Bashir R. ACS Nano. 2012; 6:441–450. [PubMed: 22165962]
31. Postma HWC. Nano Lett. 2010; 10:420–425. [PubMed: 20044842]
32. Prasongkit J, Grigoriev A, Pathak B, Ahuja R, Scheicher R. Nano Lett. 2011; 11:1941–1945. [PubMed: 21495701]
33. Saha K, Drndić M, Nikolić B. Nano Lett. 2012; 12:50–55. [PubMed: 22141739]
34. Nelson T, Zhang B, Prezhdo OV. Nano Lett. 2010; 10:3237–3242. [PubMed: 20722409]
35. Min S, Kim W, Cho Y, Kim K. Nature Nanotech. 2011; 6:162–165.
36. Sathe C, Zou X, Leburton J, Schulten K. ACS Nano. 2011; 5:8842–8851. [PubMed: 21981556]
37. Qiu H, Guo W. Appl Phys Lett. 2012; 100:83106.
38. Aksimentiev A. Nanoscale. 2010; 2:468–483. [PubMed: 20644747]
39. Comer J, Aksimentiev A. J Phys Chem C. 2012
40. Manohar S, Mantz AR, Bancroft KE, Hui CY, Jagota A, Vezenov DV. Nano Lett. 2008; 8:4365–4372. [PubMed: 19368004]
41. Johnson RR, Johnson ATC, Klein ML. Nano Lett. 2008; 8:69–75. [PubMed: 18069867]
42. Smirnov S, Vlassiouk I, Lavrik N. ACS Nano. 2011; 5:7453–7461. [PubMed: 21838311]
43. Powell M, Cleary L, Davenport M, Shea K, Siwy Z. Nature Nanotech. 2011; 6:798–802.
44. Song B, Schneider GF, Xu Q, Pandraud G, Dekker C, Zandbergen H. Nano Lett. 2011; 11:2247–2250. [PubMed: 21604710]
45. Wanunu M, Bhattacharya S, Xie Y, Tor Y, Aksimentiev A, Drndic M. ACS Nano. 2011; 5:9345–9353. [PubMed: 22067050]
46. Aksimentiev A, Heng JB, Timp G, Schulten K. Biophys J. 2004; 87:2086–2097. [PubMed: 15345583]
47. Comer J, Aksimentiev A. J Phys Chem C. 2012; 116:3376–3393.
48. Timp W, Comer J, Aksimentiev A. Biophys J. 2012; 102:L37–L39. [PubMed: 22677395]
49. Sint K, Wang B, Kral P. J Am Chem Soc. 2008; 130:16448–16449. [PubMed: 19554715]

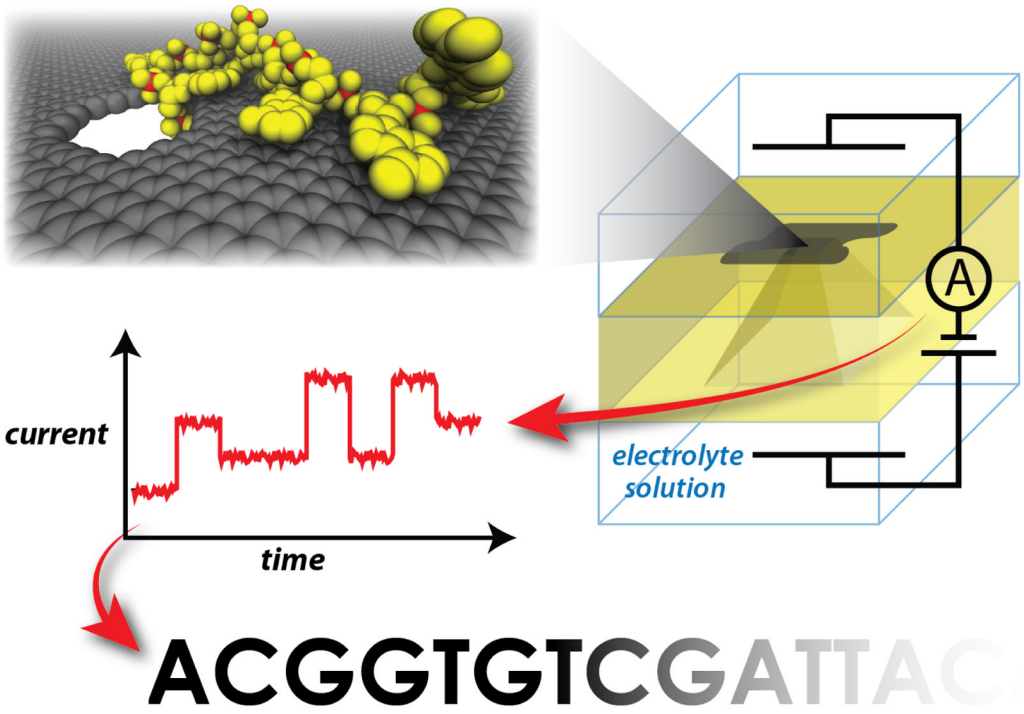

Figure 1.
Schematic of a graphene nanopore-based device for sequencing DNA. A graphene sheet containing a nanopore is placed over an aperture in a synthetic membrane. DNA is driven through the pore by a transmembrane electric field. As the DNA transits the nanopore, the ionic current is modulated by the nucleotides in the nanopore, revealing the DNA sequence.

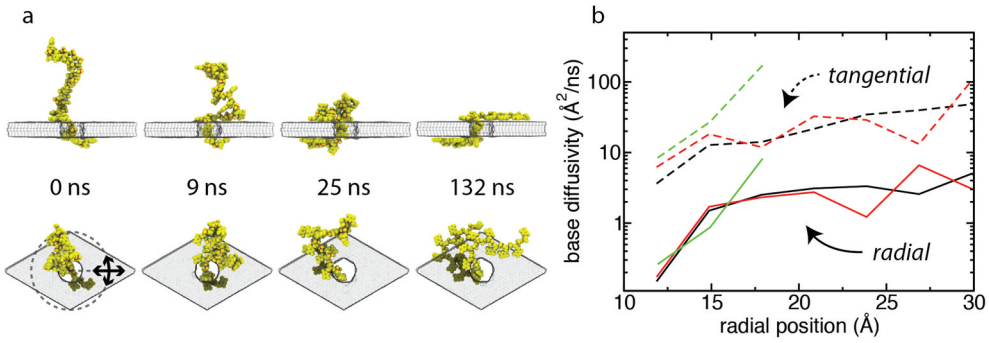

Figure 2.

Adhesion of ssDNA to the surface of a graphene membrane. (a) A typical MD simulation of ssDNA translocation through a graphene nanopore. Shown is the trajectory of poly(dT)$_{20}$ under a 500 mV bias, pore VII (see Table 1). Complete translocation data is given in Figure 3d. The snapshots in the top and bottom rows provide the side and top views of the same system. DNA atoms are shown as yellow and red spheres (red spheres indicate the phosphorus atoms); the graphene membrane is shown as a gray semitransparent surface. Water and ions are not shown. The arrows indicate the radial and tangential directions used to compute 2D diffusivities of the DNA bases. Animations M1 and M2 illustrating this trajectory are available in the Supporting Information. (b) Diffusion of bases adsorbed to the surface of one- (*green*), two- (*red*), and three-layer (*black*) membranes. The plots show the diffusivity for radial (solid lines) and tangential (dashed lines) directions.

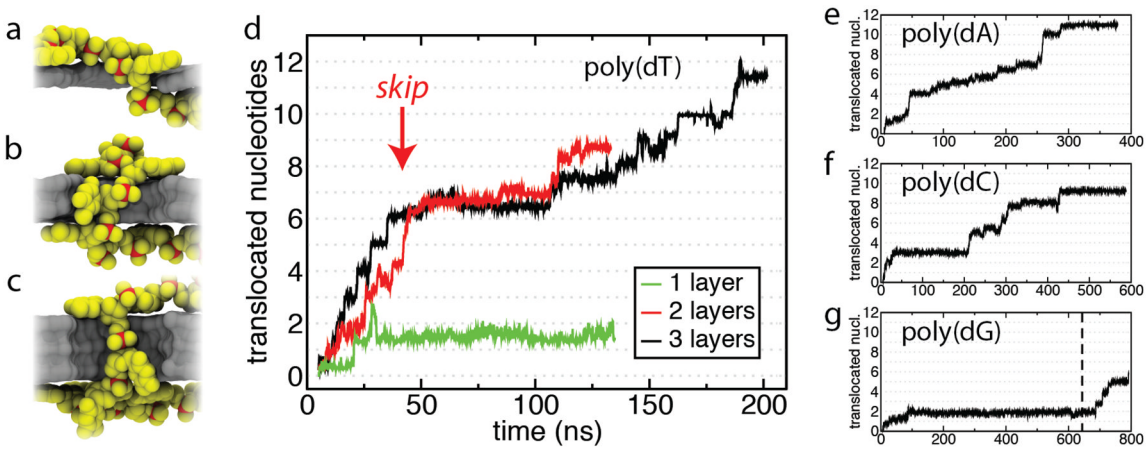

Figure 3.

DNA translocation through nanopores in one-, two-, and three-layer membranes. (a–c) Snapshots of the pore region of the systems (pores II, V, and VII) featuring one- (a), two- (b), and three-layer (c) membranes. Graphene is shown as a silver molecular surface and DNA is shown as yellow and red van der Waals spheres, where red spheres indicate the phosphorus atoms. (d) Number of translocated nucleotides as a function of simulation time for one- (pore II, *green*), two- (pore V, *red*), and three-layer (pore VII, *black*) systems. The arrow indicates base skipping: multiple bases transit the pore together. Data here are from systems containing poly(dT)$_{20}$ under a 500 mV bias. (e–g) Number of translocated nucleotides versus simulation time for pore VII (three-layer membrane) and poly(dA)$_{20}$ (e), poly(dC)$_{20}$ (f), poly(dG)$_{20}$ (g). In panel (g), the vertical dashed line indicates a bias increase from 500 mV to 800 mV.

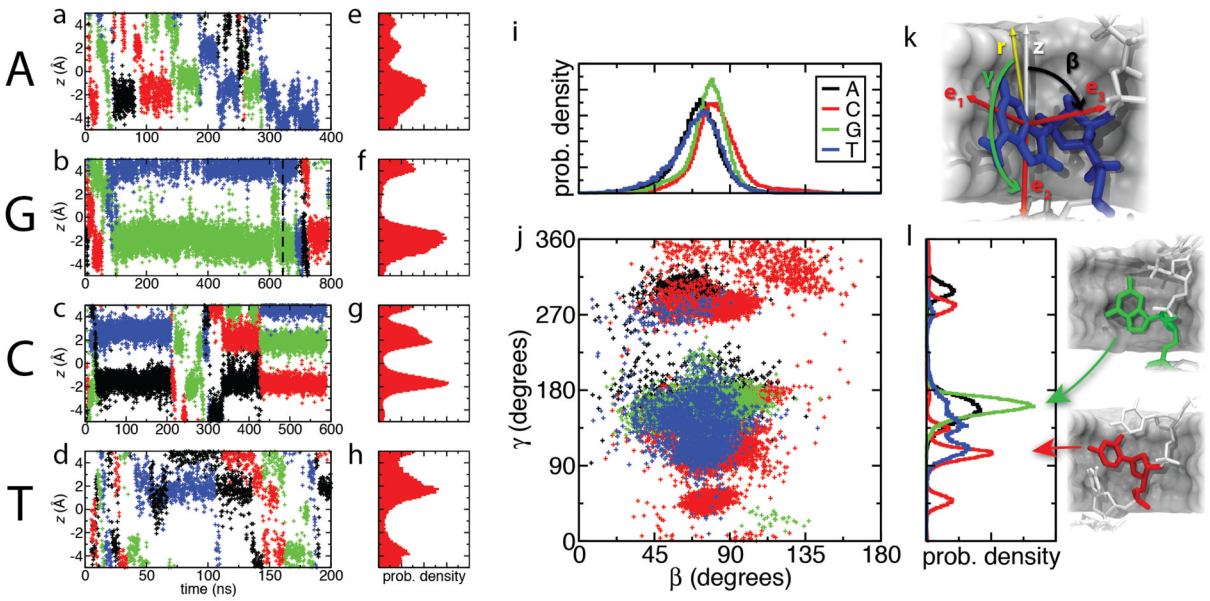

Figure 4.

Stepwise transport of ssDNA is associated with reduced conformational noise. (a–d) z coordinate of the center of mass of individual bases in poly(dA)$_{20}$ (a), poly(dG)$_{20}$ (b), poly(dC)$_{20}$ (c), and poly(dT)$_{20}$ (d) systems. To make translocation events discernible, coordinates of individual bases are plotted in black, red, green and blue. The span of the y axis ($-5 < z < 5$ Å) corresponds to the thickness of the three-layer membrane. (e–h) Normalized distributions of the bases' z coordinate. The histogram for poly(dG)$_{20}$ was computed using the MD trajectory at 800 mV (see Figure 3g). (i–l) Orientations of individual bases within pore VII in the simulations of poly(dA)$_{20}$ (*black*), poly(dC)$_{20}$ (*red*), poly(dG)$_{20}$ (*green*), and poly(dT)$_{20}$ (*blue*). The angles β and γ describe the tilt and rotation of the bases, respectively; their definitions are shown in panel (k) and in Figure S5. (j) Scatter diagram of angles β and γ. (i, l) Normalized distributions of β (i) and γ (l). The snapshots illustrate typical conformations of purine and pyrimidine bases.

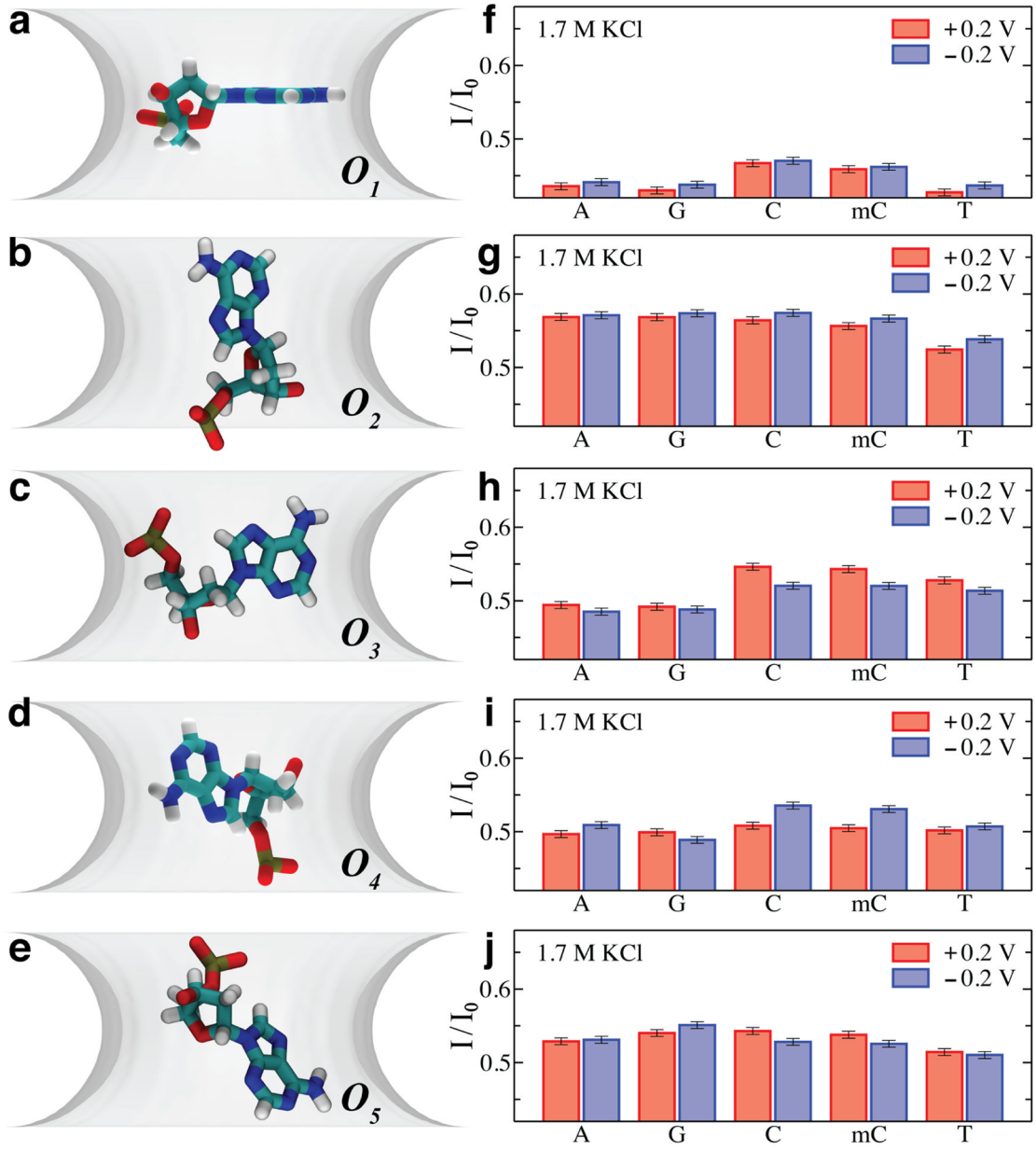

Figure 5.

ARBD simulations of the sequence dependence of the blockade ionic current. (a–e) Orientations of nucleotides considered in our BD simulations. For clarity, only one nucleotide (adenine) is shown in all-atom representation (see text). The phantom pore is drawn as a semi-transparent isosurface of its PMF map at 0.5 $k_B T$. (f–j) The relative ionic current blockade (I/I_0) for A, G, C, mC, and T nucleotides in systems with bulk KCl concentrations of 1.7 M and trans-membrane biases ± 200 mV. Error bars show 95% confidence intervals.

Table 1

Graphene nanopore systems examined using the all-atom MD method. For elliptical nanopores, major and minor radii are given. For pore VII, all simulations were carried out at 0.5 V, with the exception of the simulation of poly(dG), which was performed also at 0.8 V. The blockade current $\langle I \rangle_{seq}/I_0$ was averaged over all DNA homopolymer sequences. For pore I, the lowest [poly(dT)$_{10}$] and highest [poly(dA)$_{10}$] blockade currents among the four bases are listed.

Pore	Layers	Pore radius (Å)	Voltage (V)	I_0 (nA)	$\langle I \rangle_{seq}=I_0$
I	1	7.7	1.2	5.0	0.12–0.58
II	1	8.0	0.5	3.3	0.61
III	2	7.0 ×5.4	2	2.8	0.15
IV	2	8.0 ×6.2	0.5	1.5	0.37
V	2	8.0	0.5	2.1	0.63
VI	3	8.0 ×6.2	0.5	1.1	0.32
VII	3	8.0	0.5, 0.8	1.9	0.58